Journal of Catalysis 426 (2023) 140–152

Contents lists available at ScienceDirect

Journal of Catalysis

journal homepage: www.elsevier.com/locate/jcat

Research article

Design of bi-functional Ni-zeolites for ethylene oligomerization: Controlling Ni speciation and zeolite properties by one-pot and post-synthetic Ni incorporation

Adrián Martínez Gómez-Aldaraví, Cecilia Paris, Manuel Moliner *, Cristina Martínez *

Instituto de Tecnología Química, Universitat Politècnica de València-Consejo Superior de Investigaciones Científicas, Avenida de los Naranjos s/n, 46022 València, Spain

ARTICLE INFO

Keywords:
Olefin oligomerization
Ethylene
Zeolite
Nickel

ABSTRACT

The design of diverse Ni-zeolites has been performed attempting to control different physico-chemical properties of the zeolite supports as well as the Ni speciation to study their influence on the industrially relevant ethylene oligomerization reaction. In this sense, Ni-containing medium-pore MFI and large-pore BEA zeolites have been synthesized with different particle sizes, Si/Al molar ratios and following different Ni-incorporation strategies (one-pot versus post-synthesis). Characterization techniques reveal the preferential presence of cationic Ni^{2+} and NiO nanoclusters inside the zeolitic pores when Ni has been incorporated by post-synthesis impregnation or one-pot approaches, respectively. The presence of Ni^{2+} species, rather than other factors, mainly governs olefin oligomerization under near-ambient pressures, guiding preferentially towards C_4-C_6 olefins as main products. Crystal size, acidity and/or Ni incorporation methodology, on the other hand, play key roles under high-pressure reaction conditions, resulting in the formation of heavier olefins, especially in zeolites containing less cationic nickel, larger proportion of NiO clusters and higher Brønsted acid site density.

1. Introduction

Light olefins ($C_2^=$-$C_6^=$) are considered as key "building-blocks", intermediates for the synthesis of highly demanded organic products and fuels. Traditionally, these light olefins are mostly obtained by steam cracking processes of different feedstocks, ranging from light hydrocarbons (natural gas mixtures) to naphthas (petroleum distillates),[1,2] as well as by direct transformation of methanol through the methanol to olefins (MTO) or methanol to propylene (MTP) processes.[3] In addition to fossil fuel based processes, new and more sustainable routes to obtain these light olefins, mainly from biomass-derived products and CO_2, have received increased attention in the last years.[2,4,5].

The oligomerization of light olefins is one of the most interesting industrial pathways to produce either liquid fuels, such as gasoline, jet fuel or diesel, plasticizers or solvents, thanks to its high flexibility in terms of the starting olefin, and of the number of oligomerization steps and range of molecular weight of the final products.[6–9] Acid zeolites have been extensively employed as efficient heterogeneous oligomerization catalysts when using propylene and other olefins of higher molecular weight, and the acidity and the shape-selectivity defined by the zeolite pore topology are known to strongly influence the formation of products with specific characteristics.[6,10] On the one hand, medium pore zeolites favour the formation of linear hydrocarbons with less branched alkyl groups as compared to large pore zeolites, enhancing the production of high-quality diesel fractions.[11–13] On the other hand, highly branched bulkier products are preferentially achieved using tridirectional large pore zeolites, which may lead to faster catalyst deactivation by pore blocking.[14] Nevertheless, it has been shown that shortening the diffusion pathways within large pore zeolites, as was achieved in the case of nanosized Betas synthesized with crystal sizes in the range of 10–20 nm, allows reducing significantly the catalyst deactivation rates since large oligomers are able to diffuse out the zeolite pores before being involved in undesired consecutive reactions.[15,16].

Unlike higher olefins, very low conversions are achieved with solid acid catalysts when using ethylene as the reactant in oligomerization processes.[6] In this case, different transition metal catalysts and, specifically, Ni-containing catalysts are known to be active for ethylene dimerization and/or oligomerization.[17] In particular, Ni-containing microporous zeolites, [6,18–20] or Ni supported on mesoporous materials, such as MCM-41 [21–23] have been widely studied. The traditional nickel incorporation methods are post-synthesis ion-exchange or impregnation.

* Corresponding authors.
E-mail addresses: mmoliner@itq.upv.es (M. Moliner), cmsanche@itq.upv.es (C. Martínez).

https://doi.org/10.1016/j.jcat.2023.07.010
Received 4 May 2023; Received in revised form 12 July 2023; Accepted 15 July 2023
Available online 16 July 2023

In the presence of Ni-based catalysts, ethylene dimerization follows the Cosse-Arlman mechanism, where two ethylene molecules interact with a Ni active site forming a Ni-di-ethene complex, resulting in the formation of 1-butene (coordination step). Then, other ethylene molecules present in the media can be consecutively coordinated to the Ni sites while the 1-butene formed is still attached, stepping towards higher olefins (insertion step). Kinetic modelling and theoretical calculations have shown that the presence of acid sites in the zeolite support can play a key role for the Cosse-Arlman mechanism,[24] since their presence would help stabilizing extra-framework Ni species as divalent cations by adequately counterbalancing these positive charges with the negative charges of trivalent aluminium atoms in zeolite framework positions.[25] An alternative mechanism has been recently proposed by Moussa et al.[26] for Ni-Beta zeolites based on coupled in situ FTIR spectroscopy results and reaction kinetics, involving the coordination of ethylene to the Ni^{2+} site via π-coordination and the formation of a nickel ethenyl hydride intermediate. It is worth noting that once the olefin starts growing on the Ni active site following any of the mechanism exposed above, the resulting alkene can also be converted by the acid sites present in the zeolite support, contributing to the final product distribution with different side/consecutive reactions, such as co-oligomerization, cracking, isomerization or alkylation, among others.[6,17] Thus, developing zeolite-based catalysts with controlled acidities and/or desirable Ni/Al ratios, with the proper pore topologies and/or crystal sizes, will be highly desirable. In fact, these are some of the key properties to take into account in the design of Ni-containing bifunctional zeolite-based catalysts for enhancing the yields towards desired oligomerization products of specific size and branching degree.[27].

Despite the existing controversy in earlier studies regarding the nature of the nickel sites responsible for the activation of the ethylene molecules, i.e. Ni(0),[28] or Ni^{+},[29,30], more recent works suggest the preferential role of the divalent Ni^{2+} species, based on infrared spectroscopy employing carbon monoxide as probe molecule.[21,22,31–33] Still, not all the divalent nickel species behave in the same way, and whereas Ni^{2+} in ion exchange positions, with stronger Lewis acidity, were seen to be highly active during the first stages of the reaction they deactivate fast, leaving isolated silanol grafted Ni^{2+} cations, with milder acidity, as the sole active sites at longer times on stream.[26].

Ni species are generally incorporated in the zeolite-based supports by post-synthesis methodologies, such as ion exchange or impregnation methods.[21,22,31,32] In addition, a few works have also described the post-synthetic heterogeneization of well-defined Ni-complexes on different zeolites (i.e. Y, ZSM-5, Beta, and ITQ-2),[34–37] resulting in good catalytic performances towards the ethylene dimerization reaction. However, incorporation of Ni species via one-pot encapsulation on high-silica zeolites, their characterization and their catalytic evaluation for the ethylene oligomerization reaction has not been studied so far, even though in the last years different one-pot metal addition approaches have been shown as very efficient methodologies to improve metal dispersion and stability within microporous materials.[38,39].

Herein, we present the rational design of a set of Ni-containing zeolitic materials and their catalytic evaluation for the ethylene oligomerization reaction. Thus, two different crystalline structures have been selected (MFI and BEA), with different crystal sizes (from micron- to nano-sized particles) and chemical compositions (Si/Al molar ratios from 10 to 40) and two different Ni incorporation procedures, one-pot synthesis employing N-ligands and a traditional post-synthesis approach. The materials have been thoroughly characterized to unravel not only the physico-chemical properties of the zeolitic supports, but also the chemical state and distribution of the Ni species. Finally, the Ni-containing zeolite-based catalysts have been tested for olefin dimerization/oligomerization under low [32] and high pressure [40] conditions aiming to establish the main structure/activity relationships controlling the formation of different products, from 1-butene to larger oligomers within the range of liquid fuels.

2. Experimental section

2.1. Catalyst preparation

Three commercially available samples with MFI structure and different Si/Al molar ratios (CBV3024, Si/Al ~ 15: MFI15; CBV5524, Si/Al ~ 25: MFI25; and CBV8020, Si/Al ~ 30: MFI30) and one BEA zeolite (CP814C, Si/Al = 11: BEA11), all of them supplied by Zeolyst, have been selected as supports to post-synthetically introduce the Ni species. The Ni incorporation within the two samples with the lowest Si/Al ratio (CBV3024 and CP814C), was carried out by ion exchange employing an aqueous solution of $Ni(NO_3)_2{\cdot}6H_2O$ to theoretically introduce ~ 1 wt% Ni, fixing a liquid/solid weight ratio of 40, and maintaining the mixture under stirring overnight at 80 °C. The Ni incorporation within the commercial zeolites with higher Si/Al ratios was carried out by wet impregnation containing the required amount of $Ni(NO_3)_2{\cdot}6H_2O$ to obtain ~ 1 wt% Ni content in the material and a starting liquid/solid weight ratio of 10. In both cases, after the Ni incorporation or wet impregnation, the resultant samples were recovered, dried at 80 °C overnight and calcined at 550 °C (1 °C/min) for 4 h in air.[33].

In addition to the commercially-available zeolites, different nanozeolites with the MFI and Beta structures were also synthetized using simple organic molecules as organic structure directing agents (OSDAs) and following the methodology described by Gallego et al.[41] On the one hand, one nanosized MFI zeolite with a Si/Al molar ratio of ~ 30, nMFI30, was synthesized using *N*-butyl-*N*-methylpyrrolidinium (BMP) as OSDA under the conditions summarized in Table 1 (see detailed synthesis procedure in ref. [41]). On the other hand, two nanosized Beta zeolites with Si/Al molar ratios of ~ 15 and 30, nBEA15 and nBEA30, were synthesized using *N*-butyl-*N*-methylhexamethyleneiminium (BMH) as OSDA under the conditions summarized in Table 1 (see detailed synthesis procedure in ref. [41]). The samples were calcined at 580 °C in air to remove the OSDA molecules for 4 h using an initial heating ramp of 2 °C/min. After removing the OSDA molecules, an incipient wetness impregnation procedure to incorporate a ~ 1 wt% Ni was performed using an aqueous solution of $Ni(NO_3)_2{\cdot}6H_2O$, following the procedure described above to incorporate Ni in the commercial zeolites (Ni-nMFI30_ps, Ni-nBEA15_ps and Ni-nBEA30_ps). The Ni-containing zeolites were finally calcined at 550 °C for 4 h in air using an initial heating ramp of 1 °C/min.

The one-pot Ni-containing nanosized MFI and Beta samples were obtained employing the same synthesis conditions described above for the Ni-free nanozeolites, but including the required amount of Ni in the synthesis gels to achieve a 1 %wt Ni in the resultant materials (Ni source: $NiCl_2{\cdot}6H_2O$, ≥97% Sigma-Aldrich) and ethylenediamine (reagent grade, Sigma-Aldrich) as complexing ligand. The precise gel compositions and synthesis conditions are detailed in Table 1 (see Ni-nMFI30_op, Ni-nBEA15_op and Ni-nBEA30_op). The final solids were recovered by filtration, washed with distilled water, and dried overnight at 80 °C. After that, the solids were calcined at 550 °C in air for 4 h using an initial heating ramp of 1 °C/min.

2.2. Characterization

Powder X-Ray diffraction (PXRD) measurements were performed employing a multisample holder Philips X'Pert diffractometer fitted with a graphite monochromator, running at 35 mA and 40 kV and a Cu Kα radiation of 0.1542 nm of wavelength.

The chemical composition of the materials was determined by Inductively Coupled Plasma - Optimal Emission Spectroscopy (ICP-OES) using a Thermo-Scientific iCAP PRO spectrometer after dissolving the solid samples in an acid mixture of HNO_3: HCl: HF (1:3:1 volumetric ratio).

The morphologies and crystal sizes of the different zeolites as well as the presence/absence of Ni particles on the external surface of the zeolite crystals were studied by High Resolution Field Emission

Table 1
Theoretical molar composition of synthesis gels. The employed OSDA molecules for the syntheses of the nanosized MFI and BEA zeolites were *N*-butyl-*N*-methylpyrrolidinium (BMP) and *N*-butyl-*N*-methylhexamethyleneiminium (BMH), respectively.

	SiO_2	Al_2O_3	OSDA	EDA	$NiCl_2$	T (°C)	t (d)	Stirring
nMFI30	1	0.017	0.4 (BMP)	0	0	150	10	Yes
Ni-nMFI30_op	1	0.017	0.4 (BMP)	0.11	0.01	150	10	Yes
nBEA15	1	0.033	0.4 (BMH)	0	0	150	14	No
Ni-nBEA15_op	1	0.033	0.4 (BMH)	0.11	0.01	150	14	No
nBEA30	1	0.017	0.4 (BMH)	0	0	150	14	No
Ni-nBEA30_op	1	0.017	0.4 (BMH)	0.11	0.01	150	14	No

Scanning Electron Microscopy (HR-FESEM) employing a ZEISS GeminiSEM 500 microscope (ZEISS-Oxford Instruments) fitted with a Backscattered detector. Crystal size distribution of the nanozeolites was determined based on images obtained by TEM (bright field), performing around 60 measurements on different transmission microscopy images and considering only isolated crystallites.

The presence/absence of encapsulated Ni clusters within zeolite crystals was studied by High-Angle Annular Dark-Field Scanning Transmission Electron Microscopy (HAADF-STEM) employing a JEOL JEM-2100F (JEOL-Oxford Instruments) running at 200 kV.

The textural properties of the zeolitic materials were obtained from their N_2 adsorption isotherms, measured in an ASAP2000 device (Micrometrics) at −196 °C after being degasified at 400 °C overnight, by employing the Brunauer-Emmet-Teller (BET) method.

The acidity of the materials was determined by using Fourier Transformed Infrared Spectroscopy in a Nicolet 710 FTIR device and using pyridine as the probe molecule. Self-supported wafers (10 mg/cm^2) of the samples were previously degasified overnight at 400 °C and dynamic vacuum (10^{-6} mbar). After activation, the base spectrum was recorded and pyridine vapour (6.5 10^2 Pa) was admitted in the IR cell and adsorbed onto the zeolite. Desorption of pyridine was performed under vacuum over three consecutive one-hour periods of heating at 150, 250 and 350 °C, each of them followed by the IR measurement at room temperature. All the spectra were normalized to the area of the corresponding Si-O overtones (1755–2100 cm^{-1}). The amount of Brønsted (BAS) and Lewis acid sites (LAS) was determined from the intensities of the bands at ca. 1545 and 1450 cm^{-1}, respectively, using the molar extinction coefficients given by Emeis.[42].

The nature and oxidation states of the Ni species in the samples were studied by FTIR spectroscopy using CO as probe molecule. The spectra were registered by a Nexus (Thermo) 8700 FTIR spectrometer employing a DTGS detector and measuring at 4 cm^{-1}. The calcined samples were pressed to self-supported wafers of 10 mg/cm^2, and thermally activated at 550 °C for 6 h (heating ramp of 5 °C/min). Ni speciation was assessed by titration with CO upon cooling the sample to −176 °C under dynamic vacuum of 10^{-5} mbar and introducing the CO doses increasing its partial pressure from 0.1 to 2 mbar.

The reducibility of the metal species was studied by Temperature Programmed Reduction in H_2 (H_2-TPR) using a Micrometrics Autochem 2910 instrument. The samples were exposed to a gas flow of 50 mL/min (10%H_2, 90%Ar) and temperature was increased until 900 °C at a rate of 10 °C/min.

2.3. Catalytic tests

Catalytic tests were performed in a 10 mm internal diameter stainless steel fixed-bed reactor. Zeolites were pelletized, crushed and sieved to obtain a particle size between 0.2 and 0.4 mm and diluted in all cases in SiC (0.6–0.8 mm particle size) to a total bed volume of 4.0 mL. Prior to the catalytic test, the catalysts were activated in N_2 flow (53.8 mL/min) increasing temperature to 550 °C (heating ramp of 5 °C/min), maintaining it for 6 h and, finally, cooling down to the reaction temperature. [40].

Catalytic tests were performed at both low and high pressures (2.5 and 35 bar, respectively), using similar reaction conditions to those reported previously in the literature by Gounder et al.[32] and Moon et al.,[40] respectively (detailed reaction conditions can be found in Table 2).

The outlet stream was vaporized and analysed on-line with an Agilent 7890B gas chromatograph equipped with two independent channels. In a first channel, the unreacted ethylene and the products obtained were separated in a 30 m × 320 μm × 0.25 μm HP5 column and quantified by means of a FID detector. Ethylene and N_2 were separated in a second channel provided with a 30 m × 320 μm 12 μm HP-Plot Molesieve, a 30 m × 320 μm × 20 μm HP-Q-plot, and a TCD detector.

3. Results

3.1. Synthesis and characterization of the different Ni-containing zeolites: one-pot versus post-synthetic Ni incorporation

As stated above, the oligomerization of ethylene to heavier hydrocarbons can be catalyzed by bifunctional Ni-containing acid supports. In order to activate the olefin and to achieve the formation of different oligomers, controlling both Ni speciation and the support properties (acidity and accessibility) has been revealed to be determinant. Recently, we have reported unique catalytic performances when employing ultra-small nanosized zeolites of 10–15 nm as acid catalysts for the oligomerization of larger light olefins, i.e. 1-pentene, with improved resistance against catalyst deactivation and higher yields towards liquid products within the range of gasoline and diesel.[15,16] Considering this, we propose studying these nanosized acid zeolites as supports to incorporate the required Ni species to undergo the ethylene oligomerization reaction. Moreover, the incorporation of Ni by means of different post-synthetic and one-pot synthesis methods will enable evaluating the influence of the Ni speciation.

First, a nanosized MFI sample with a Si/Al molar ratio of 30 (nMFI30) and two nanosized BEA zeolites with Si/Al molar ratios of 15 and 30 (nBEA15 and nBEA30, respectively), were synthesized using the recent methodology described by Gallego et al. employing simple organic molecules as OSDAs (see experimental section for synthesis details).[41] The resultant as-prepared MFI and BEA samples present the characteristic PXRD patterns of these structures (see Fig. 1) and, as expected, the presence of broad, low intensity diffraction peaks suggests the crystallization of these materials in their nanosized forms. In fact, the inspection of these as-prepared materials by FE-SEM microscopy clearly shows the nano-range dimensions of their particles, with average primary particle sizes of ~ 10 nm (see nMFI30, nBEA15 and nBEA30 in Figures S1 and S2). A thorough analysis of TEM (bright field) images confirms average crystal sizes around 10 nm for all the nanozeolites (see Figures S3 and S4).

The ICP analyses of these three materials confirm final Si/Al molar ratios in the solids analogous to those given by the composition of the synthesis gels (see nMFI30, nBEA15 and nBEA30 in Tables 1 and 3). After their calcination in air to remove the occluded OSDA molecules, around ~ 1 wt% of Ni has been incorporated by incipient wetness impregnation, as confirmed by ICP analyses (see Ni-nMFI30_ps, Ni-nBEA15_ps and Ni-nBEA30_ps in Table 3).

In order to see the influence of the metal incorporation procedure on the final metal speciation within the nanosized zeolites, we have also

Table 2
Reaction conditions employed for the catalytic tests.

	Pressure (bar)	Temperature (°C)	WHSV (hr^{-1})	m_{cat} (mg)	Q_{total} (mL/min)	$\%N_2$ vol	$\%C_2H_4$ vol
Gounder et al. [32]	2.5	180	16.3	63	600	97.5	2.5
Moon et al. [33,40]	35	200	2.1	500	100	85	15

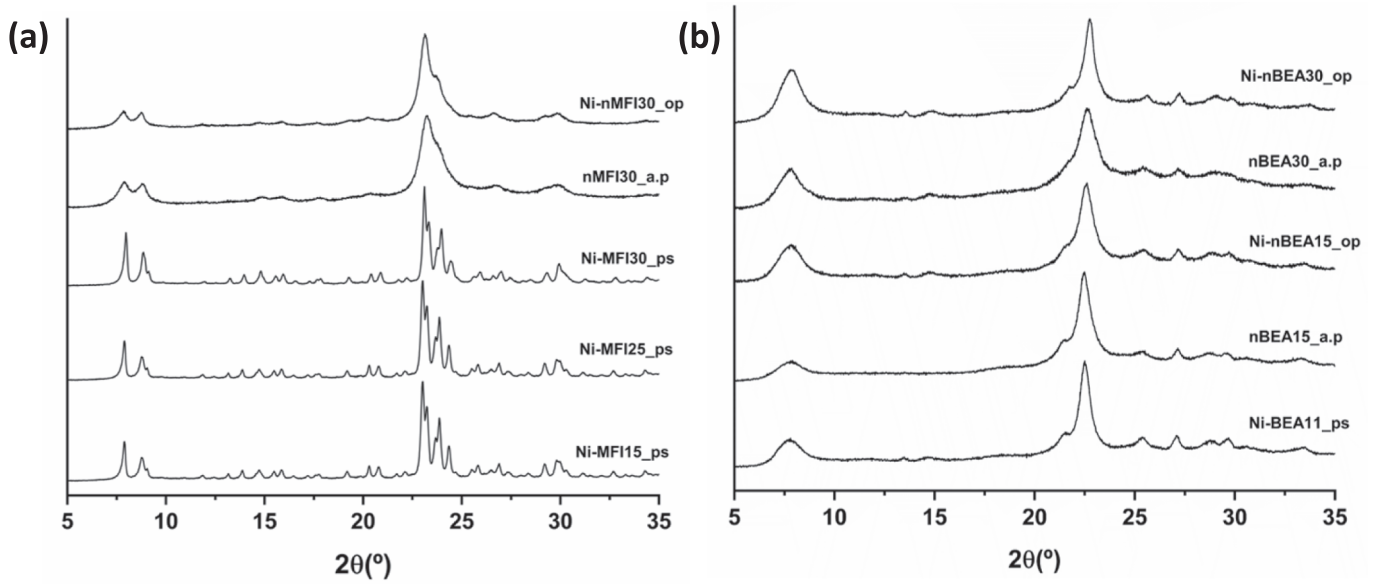

Fig. 1. PXRD patterns of the different MFI (a) and BEA (b) zeolites considered in the present study.

Table 3
Physico-chemical properties of the different Ni-containing zeolite catalysts.

Catalyst[a]	Si/Al	%Ni	BET Area (m^2/gr)	Micropore Area (m^2/gr)	External surface (m^2/gr)	Micropore Volume (cm^3/gr)
Ni-MFI15_ps (CBV3024)	14.1	0.92	411	369	42	0.16
Ni-MFI25_ps (CBV5524)	25.9	1.1	414	369	45	0.16
Ni-MFI30_ps (CBV8020)	29.0	1.1	408	357	51	0.15
Ni-nMFI30_ps	24.3	1.1	523	280	243	0.11
Ni-nMFI30_op	28.1	1.2	528	320	208	0.13
Ni-BEA11_ps (CP814C)	10.8	1.1	633	441	192	0.18
Ni-nBEA15_ps	14.0	0.95	590	331	259	0.14
Ni-nBEA15_op	12.9	1.2	714	403	311	0.17
Ni-nBEA30_ps	22.2	1.2	668	358	310	0.15
Ni-nBEA30_op	21.0	1.3	744	433	311	0.18

[a] ps: post-synthesis, op: one-pot.

contemplated the one-pot synthesis of Ni-containing nanosized MFI and Beta samples by introducing a simple Ni-complex (Ni-ethylenediamine, Ni-EDA) during their hydrothermal syntheses (see experimental section and Table 1 for details). The as-prepared Ni-nMFI30_op, Ni-nBEA15_op and Ni-nBEA30_op present similar PXRD patterns as compared to their as-prepared Ni-free zeolites counterparts (see Fig. 1), suggesting that the addition of the Ni-EDA complex to the synthesis gels does not affect the zeolites crystal size. This is confirmed by FE-SEM and bright field TEM microscopy, and the images shown in Figures S1 to S4 evidence their crystallization as primary particles with sizes ~ 10 nm. In addition, according to the ICP analyses, the one-pot Ni-nanozeolites not only maintain similar Si/Al molar ratios as compared to their Ni-free counterparts, but also present final Ni content close to 1 wt%, comparable to the analogous nanosized samples where Ni has been post-synthetically incorporated (see Table 3). The presence of the Ni-complex in the gel of the one-pot synthesized Ni-zeolites could have an influence on the degree of Al incorporation in framework or extra-framework position. According to our previous work,[41] all the Al was tetrahedrally coordinated in the as-synthesized zeolite structure when a nanosized Beta with Si/Al = 15 was prepared under comparable conditions in the absence of the Ni precursor, and after calcination at 580 °C around 80% of this Al remained in the framework. Comparing the ^{27}Al MAS NMR spectra of the Ni-free and Ni-containing nBEA15 prepared in this work (see Figure S5), the proportion of extra-framework Al is 25% and 19%, respectively, results that suggests that the presence of Ni in the synthesis gel partially stabilizes the zeolite framework dealumination. A possible explanation is the formation of cationic Ni species during the calcination process, which will remain in charge compensation sites as will be discussed later.

For comparison purposes, different commercially available samples with MFI (MFI15: CBV3024, MFI25: CBV5524 and MFI30: CBV8020) and BEA (BEA11: CPC814C) topologies have been selected, all of them with Si/Al molar ratios comparable to those of the nanosized zeolites (see Table 3) but with larger crystal sizes (see Figures S1 and S2). On the one hand, the three commercial MFI samples have similar crystal sizes of 0.1–0.2 μm (see Figure S1) and Si/Al molar ratios ranging from 15 to 30 (Si/Al ~ 15: MFI15; Si/Al ~ 25: MFI25; Si/Al ~ 30: MFI30, see Table 3). On the other hand, the commercially available Beta zeolite has a Si/Al molar ratio of ~ 11 (see BEA11 in Table 3), slightly lower but close to the one measured for the commercial MFI15 sample. FE-SEM images clearly reveal that the average size of the primary particles in BEA11 is ~ 25–30 nm (see Figure S2), which is also in the nanosized range but

still larger than those achieved by the method described by Gallego et al. (10–20 nm).[15,16,41] A ~ 1 wt% Ni has also been incorporated post-synthetically within these commercial zeolite supports (see in Table 3).

As expected, because of their smaller crystal size (see Figures S1 and S2), the external surface areas of the Ni-nMFI and Ni-nBEA samples are remarkably higher than those of the commercial ZSM-5 and Beta zeolites (see Table 3), with values up to ~ 200–250 m^2/g for the Ni-containing nanosized MFI samples or ~ 260–310 m^2/g for the ultra-small Ni-nBEA15 samples, as compared to the ~ 40–50 m^2/g or ~ 190 m^2/g obtained for the commercial-based MFI or BEA11 samples, respectively.

The Brønsted and Lewis acidities of the different Ni-zeolites, determined by FT-IR combined with pyridine adsorption and desorption at different temperatures, are summarized in Table 4 and the spectra in the pyridine region are compared in Fig. 2. All samples present the bands at 1545 and 1455 cm^{-1} assigned to the basic probe protonated by Brønsted acid sites and coordinated to Lewis acid sites, respectively. Regarding the commercial zeolites, post-synthesis incorporation of Ni results in an important decrease of the Brønsted acidity and a sharp increase of the Lewis acid band (see Fig. 2 and Table 4), especially for the zeolites with lower Si/Al ratio (Ni-MFI15_ps and Ni-BEA11_ps). This suggests that a large proportion of Ni has been incorporated as cationic Ni species in ion-exchange positions, reducing the Brønsted acidity as compared to the parent zeolites in protonic form.[27,43] In addition, these samples also present a band centered at 1610 cm^{-1}, assigned in the literature to pyridine coordinatively bonded to Ni^{2+} cations (see Fig. 2).[33] The same trends are observed for the post-synthesis impregnation of Ni on the nanozeolites (see for instance Ni-nMFI_30_ps and Ni-nBEA_30_ps in Fig. 2). However, Ni incorporation by direct synthesis to the nanocrystalline MFI and BEA zeolites with higher Si/Al ratios (Ni-nMFI30_op and Ni-nBEA30_op) does not modify the Brønsted acid site density nor the Lewis acid site density of the final samples in a significant manner. These results, together with the lower intensity of the Ni^{2+} band at 1610 cm^{-1} in the corresponding spectra (see Fig. 2), suggest that the direct Ni incorporation might result preferentially in the formation of NiO species instead of favouring the formation of extra-framework cationic Ni species in charge compensation sites. Finally, an intermediate behaviour is observed for the Ni-containing nanosized Beta with higher Al content (Ni-nBEA15_op). In this case, Brønsted acidity is not reduced as compared to the Ni-free zeolite but the intensity of the band corresponding to cationic Ni^{2+} species is comparable to that of the Ni-impregnated samples and its Lewis acidity is increased, suggesting the existence of both NiO and cationic Ni^{2+} species. The presence of cationic Ni species was already suggested by the higher stabilization towards dealumination observed for Ni-nBEA15_op, synthesized in the presence of the Ni-EDA complex. The presence of part of the cationic Ni^{2+} species as grafted to isolated silanols instead of in charge compensation sites would explain the preservation of the Brønsted acidity while increasing the Lewis acid site density.

It is worth noting that the different Ni speciation in the samples prepared by one-pot or post-synthetic methods is observed for both MFI and Beta zeolites. This allows concluding that the post-synthetic incorporation will provide more cationic Ni^{2+} species in charge compensation sites whereas the direct incorporation may favour the formation of NiO species, independently of the pore topology of the support.

To further analyse and unravel the nature of the Ni species in the prepared materials, selected samples have been characterized by FTIR-spectroscopy using CO as probe molecule. Two commercially available Ni-free MFI samples with different Si/Al molar ratios have been first studied (see MFI15 and MFI30 in Fig. 3a and 3c). These bare MFI samples mainly present two bands at ca. 2175 and 2138 cm^{-1}, which have been assigned in the literature to CO adsorbed on Brønsted sites and CO condensed inside the zeolite pores ('liquid-like' behaviour), respectively.[44] Moreover, the commercial MFI sample with less Al content, MFI30, shows an additional contribution at 2160 cm^{-1}, which can be assigned to CO attached to silanol groups.[45] After post-synthesis incorporation of Ni, the IR-spectra of the Ni-MFI sample with more Al shows the appearance of two bands at 2204 cm^{-1} and 2212 cm^{-1} (see Fig. 3a), which have been assigned to the interaction of CO with Ni^{2+} species in exchangeable positions,[21,45] whereas the IR-spectra of the Ni-MFI sample with less Al shows the appearance of a band at 2192 cm^{-1} (see Fig. 3c), assigned to Ni^{2+} grafted to the silanols within the zeolite structure.[21,45] This is even more clear when comparing the spectra after adsorption of a CO monolayer (see Figure S6). When incorporated to a sample with high Brønsted acid site density such as MFI15-H, nickel is preferentially located as Ni^{2+} in charge compensating sites (band at 2212 cm^{-1}). As the amount of Brønsted acid sites decrease and less ion-exchange sites are available, the amount of Si-OH grafted Ni^{2+} and NiO nanoparticles increases (bands at ~ 2190 and ~ 2150 cm^{-1}). In both cases, a significant decrease of the bands associated to the Brønsted acid sites is clearly observed in Fig. 3, in good agreement with the FTIR-pyridine experiments.[46] Regarding the nanosized MFI samples, the spectrum of the Ni-free nMFI30 zeolite and that of the one-pot synthesized Ni-nMFI30_op are very similar (see Fig. 3d). Still, the intensity of the band at ~ 2175 cm^{-1} in the Ni-nMFI30_op sample is slightly increased as compared to the parent nMFI30. This band, assigned to the interaction of CO with the Brønsted acid sites of the zeolite, has also been related to the presence of NiO species by different authors,[45] and its increase in the case of the Ni-nMFI30_op sample would confirm the presence of these species, in good agreement with the appearance of a band at ~ 2150 cm^{-1} at low CO coverages (see Fig. S6d). Moreover, this sample also presents a small fraction of dispersed Ni^{2+} species attached to Si-OH species, as can be deduced from the increase in the band at ca. 2192 cm^{-1}, in both Fig. 3d and Fig. S6d. In contrast, the spectrum of the Ni-nMFI30_ps shows a remarkable decrease of the band at 2175 cm^{-1}, associated to the Brønsted acid sites (see Fig. 3d) in good agreement with the FTIR-pyridine results (see Fig. 2) and the appearance of a characteristic band at 2168 cm^{-1} (see Fig. 3d), which has been assigned to Ni^{+}–CO species.[47] Different authors have proposed that the formation of these Ni^{+} species could be explained by a self-reduction phenomena during the high temperature and high-vacuum pre-treatments.[21,44,48].

Similar trends are observed for the BEA-based materials (see Fig. 4 and Fig. S6e and f). The Ni-free nBEA30 shows the presence of two signals centred at 2175 and 2160 cm^{-1} that can be assigned to the CO interacting with the Brønsted acid sites and silanol groups, and a third signal centred at 2138 cm^{-1} associated to the "liquid-like" CO adsorbed

Table 4
Acidity of the different Ni-free and Ni-containing zeolites as determined by FT-IR combined with pyridine adsorption–desorption.

Sample[a]	Brønsted acidity[b] (μmol Pyr/gr cat)	B_{350}/B_{150} [c]	Lewis Acidity[b] (μmol Pyr/gr)	L_{350}/L_{150} [c]
MFI15-H	548	0.7	16	1.0
Ni-MFI15_ps	104	0.4	477	0.2
MFI25-H	461	0.8	38	0.8
Ni-MFI25_ps	153	0.9	143	0.6
MFI30-H	372	0.8	38	0.6
Ni-MFI30_ps	200	0.6	208	0.3
nMFI30-H	382	0.8	133	0.6
Ni-nMFI30_ps	259	0.5	406	0.5
Ni-nMFI30_op	400	0.7	120	0.7
BEA11-H	469	0.5	269	0.8
Ni-BEA11_ps	74	0.1	366	0.5
nBEA15-H	345	0.6	227	0.8
Ni-nBEA15_ps	146	0.5	306	0.6
Ni-nBEA15_op	355	0.5	346	0.8
nBEA30-H	244	0.7	172	0.7
Ni-nBEA30_ps	169	0.4	352	0.6
Ni-nBEA30_op[a]	272	0.5	166	0.8

[a] H: Ni-free acid form, ps: post-synthesis, op: one-pot.
[b] μmol pyr retained after desorption treatment at 150°C.
[c] ratios of μmol pyr retained after desorption treatments at 350 and 150°C.

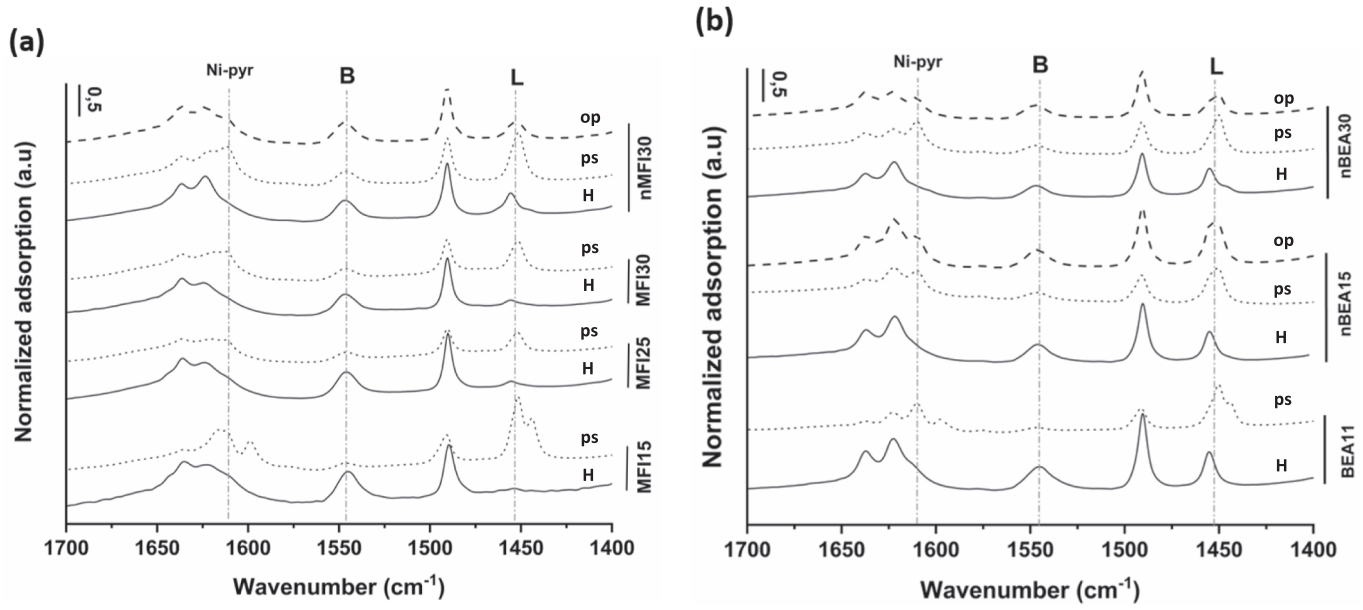

Fig. 2. FTIR-pyridine spectra after the desorption treatment at 150ºC for the MFI (a) and BEA-type (b) materials, including parent zeolites (H, straight trace), and the Ni-containing zeolites where Ni has been added post-synthetically (ps, dot trace) or via one-pot (op, dash trace).

inside the pores. However, unlike what occurs with the nMFI30 samples, when Ni is incorporated by post-synthesis treatments to the nBEA30 sample, there is no decrease of the band associated to the Brønsted acid sites (see Fig. 4b). The reason for this is that the decrease in Brønsted acid site density observed by the adsorption of pyridine is compensated, in this case, by the formation of NiO species, as their interaction with CO would lead to a band at the same wavelength. This is confirmed by the appearance of this band a low doses of CO. The appearance of a large contribution at 2204 cm^{-1} suggests that an important fraction of the Ni species could be present as Ni^{2+} grafted to isolated silanol groups from the zeolite structure, as proposed by Martínez et al.[45] A clear increase of the band at 2137 cm^{-1} in both Ni-nBEA30_op and Ni-nBEA30_ps is observed (see Fig. 4b), which could be explained by the presence of the Ni^{+}(CO) complex that would also agree with the presence of a weak shoulder at 2109 cm^{-1}.[44,49] In addition, the Ni-nBEA30_op sample shows an increase of the band at 2175 cm^{-1} (see Fig. 4b), associated to both Brønsted acid sites and NiO species, explained by the presence of the latter according to the presence of the corresponding band at ~ 2150 cm^{-1} in Fig. S6f), as described above for the Ni-nMFI30_op sample (see Fig. 3d). Thus, from the FTIR-spectroscopy study using CO as probe molecule, we could conclude that the different Ni incorporation methods in both MFI and BEA-type structures preferentially lead to the formation of a larger amount of NiO species or cationic Ni species when performing one-pot or post-synthetic incorporation methods, respectively.

The interaction of the nickel species with the different –OH groups discussed so far is confirmed when comparing the FTIR spectra in the Si-OH stretching region (see Figure S7). Indeed, post-synthesis impregnation of nickel on commercial MFI (micron-sized) zeolites results not only in a decrease of the acid hydroxyls, responsible for the Brønsted acidity of the zeolite (~3600 cm^{-1}), but also in a decrease of the bands assigned to internal isolated silanols (3738 cm^{-1}) [50,51] whereas the one corresponding to external isolated silanols (3746 cm^{-1}) is not affected. This agrees with the low T CO adsorption results, confirming that part of the cationic nickel species are interacting with isolated silanols. Moreover, it evidences that Ni^{2+} is grafted preferentially to isolated silanols located inside of the microporous structure.

In the case of both MFI and BEA nano-zeolites, a single band is observed in the isolated silanol region (see Fig. S7). Still, in the case of the Ni-nMFI30_ps catalyst, this band is significantly decreased as compared to its Ni-free counterpart and the acid hydroxyl band is no longer observed. For the Ni-nBEA15 samples a clear decrease of the isolated silanol and the acid hydroxyls bands is observed for both, post-synthesis and one-pot synthesis nickel incorporation, although larger for the sample prepared by post-synthesis impregnation. This sample presents, therefore, both type of Ni^{2+} species in significant and comparable proportion, as mentioned before. Finally, the differences when comparing the Ni-free and Ni-containing nBEA30 samples are not so significant, although post synthesis incorporation of the metal reduces both isolated silanols and Brønsted acid sites in a larger extend than one-pot synthesis incorporation.

In good agreement with the IR-CO results, NiO particles were not detected by FESEM on the materials surface of the Ni-containing zeolites (see Figures S1 and S2), except for some isolated particles in the case of Ni-MFI25_ps and Ni-MFI30_ps, based on the commercial ZSM-5 with Si/Al = 25 and 30. In addition, the dark field STEM images allowed confirming the presence of NiO nanoparticles in the samples in which nickel was encapsulated by one-pot synthesis, whereas they were not observed for the Ni-zeolites prepared by post-synthesis impregnation (see Figures S8 and S9).

The different Ni-containing samples have been also characterized by H_2-TPR to evaluate the reducibility of the Ni-species present. According to the literature, hydrogen consumptions at temperatures below 300 °C are associated to the reduction of external bulk NiO nanoparticles, weakly interacting with the support,[21,32,52,53] whereas reduction of cationic Ni(II) to Ni(0) has been described to occur in a wide temperature range, from 360 to ~ 600 °C, depending on the cation location, on the zeolite structure and/or interaction with the zeolite.[21,32,48,52,53] All the Ni-containing samples present reduction peaks within this intermediate temperature window, responsible for most of the hydrogen consumption and with the maximums shifted to higher temperatures in the case of the post-synthesis Ni incorporation (see Fig. 5 and Table S1), indicating a stronger interaction of the Ni^{2+} cations with the zeolite. On the other hand, the Ni-zeolites obtained by one-pot synthesis present an important H_2 consumption in the low temperature range, assigned to NiO nanoparticles on the external surface, and a main reduction peak at temperatures above 600 °C, assigned to the reduction of small encapsulated NiO nanoparticles strongly interacting with the

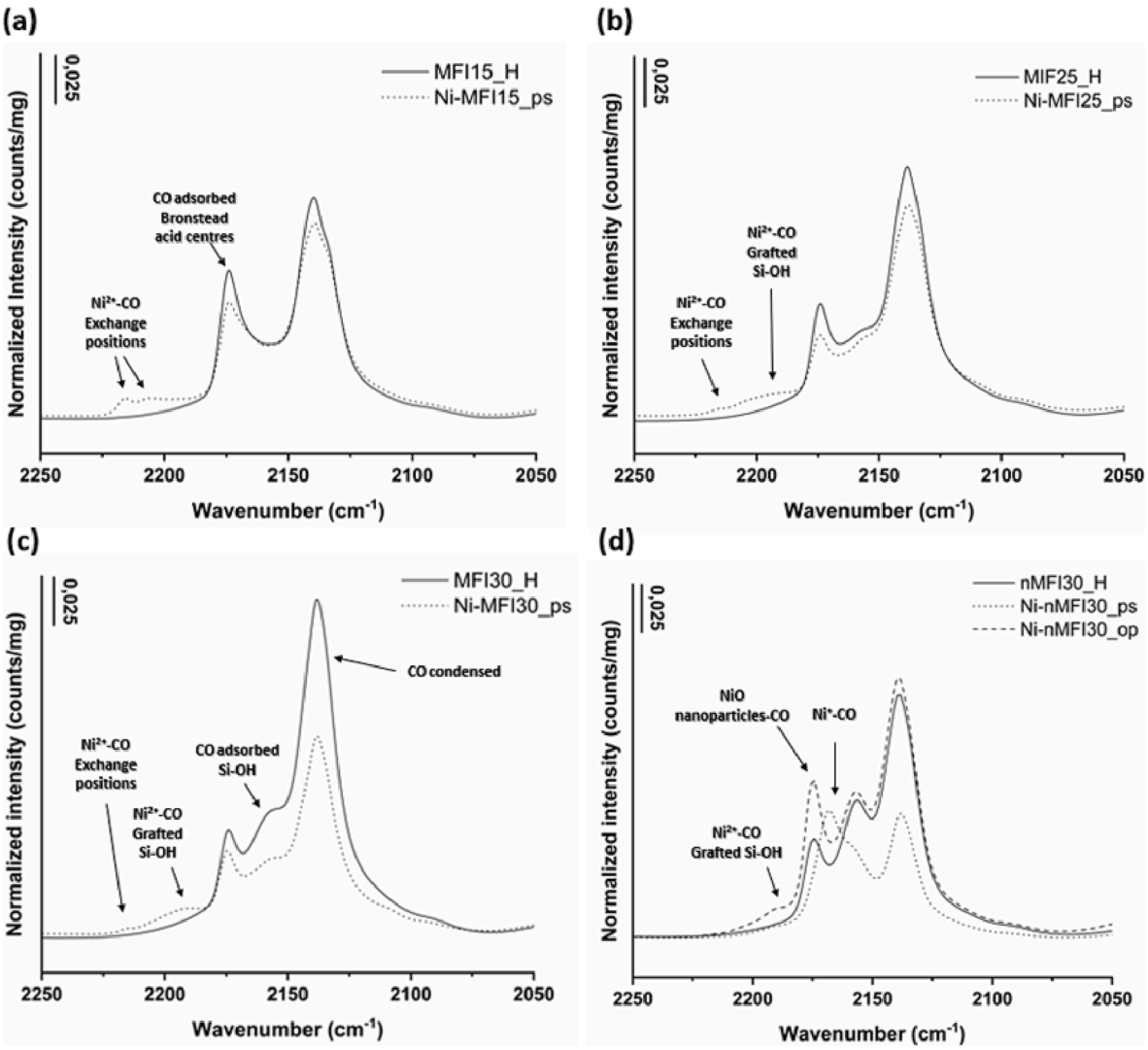

Fig. 3. FTIR spectra using CO as probe molecule at CO saturation for the Ni-containing commercial MFI zeolites (a, b, c), and synthetized nanosized MFI (d). The panels include the parent zeolites (solid trace) and the Ni-containing zeolites where Ni has been added via post-synthetic (dot trace) and/or one-pot methods (dash trace).

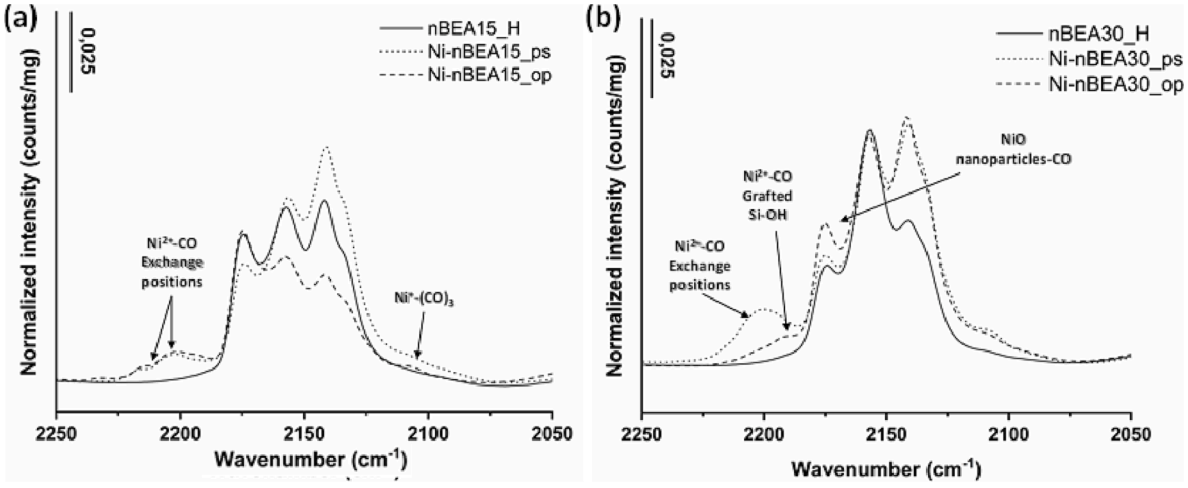

Fig. 4. FTIR spectra using CO as probe molecule at CO saturation for the Ni-containing nanosized Beta zeolites: nBEA15 (a) and nBEA30 (b). The panels include the parent zeolites (solid trace) and the Ni-containing zeolites where Ni has been added via post-synthetic (dot trace) and/or one-pot methods (dash trace).

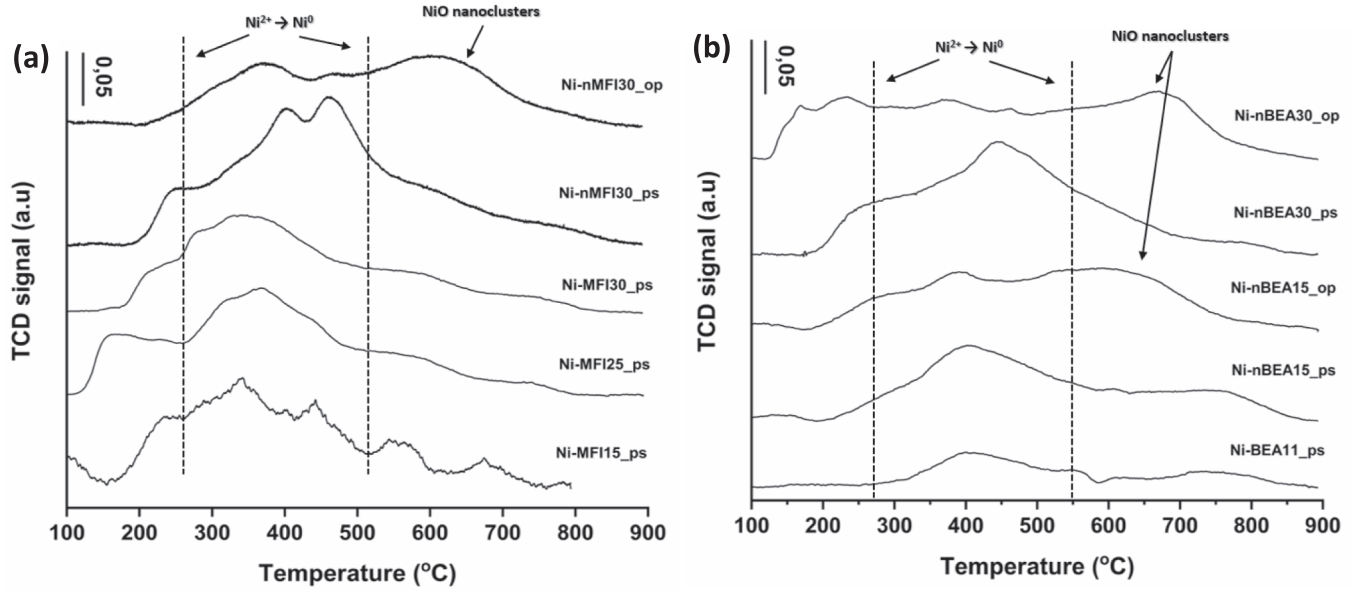

Fig. 5. H_2-TPR profiles for all the Ni-containing MFI-type (a) and BEA-type (b) materials.

support as recently reported by Li et al. when encapsulating Ni species by one-pot methods.[54] The relative H_2 consumption in the high temperature range observed for some of the post-synthesis impregnated zeolites could also be related to the presence of highly dispersed cationic nickel species, strongly interacting with the zeolitic support.[21] Thus, H_2-TPR results also correlate with those obtained by IR spectroscopy using pyridine and CO as probe molecules, and allow us to conclude that, depending on the synthesis method employed, different final Ni states can be obtained. Based on this and on the differences observed in the Brønsted acid site density of the Ni-zeolites, different catalytic behaviour could be expected for these materials.

3.2. Ethylene oligomerization: Effect of the Ni species and physico-chemical properties of zeolite supports on activity and product selectivity

The performance of the Ni-zeolites with different Ni speciation and physico-chemical properties of the microporous supports (i.e., pore topology, crystal size and acidity) as catalysts for the oligomerization of ethylene has been evaluated under two sets of reaction conditions (see Table 2). In a first approach, oligomerization has been performed under near ambient pressure, low partial pressure and high space velocity, conditions under which high selectivity to butenes is expected,[32] even in the presence of Brønsted acid sites. In a second approach, catalytic behaviour has been compared working at higher total pressure, lower space velocity and higher ethylene concentration in the feed. In this case, the formation of higher oligomers, which could be considered as liquid fuels, will be favoured.[33,40].

Fig. 6 shows the activity of the MFI and BEA based catalysts compared under near-atmospheric pressure conditions. The first thing to be noted is that in all cases the activity after the first 50 min on stream remains constant with TOS. However, an activity loss is observed at shorter times on stream (<50 min), higher for the medium pore ZSM-5 than for Beta-based catalysts with comparable Si/Al ratio and preparation procedure, and more pronounced for zeolites with higher Al content, especially in the case of MFI (see Fig. 6a and Table S2). This deactivation observed during the first stages of the reaction was related

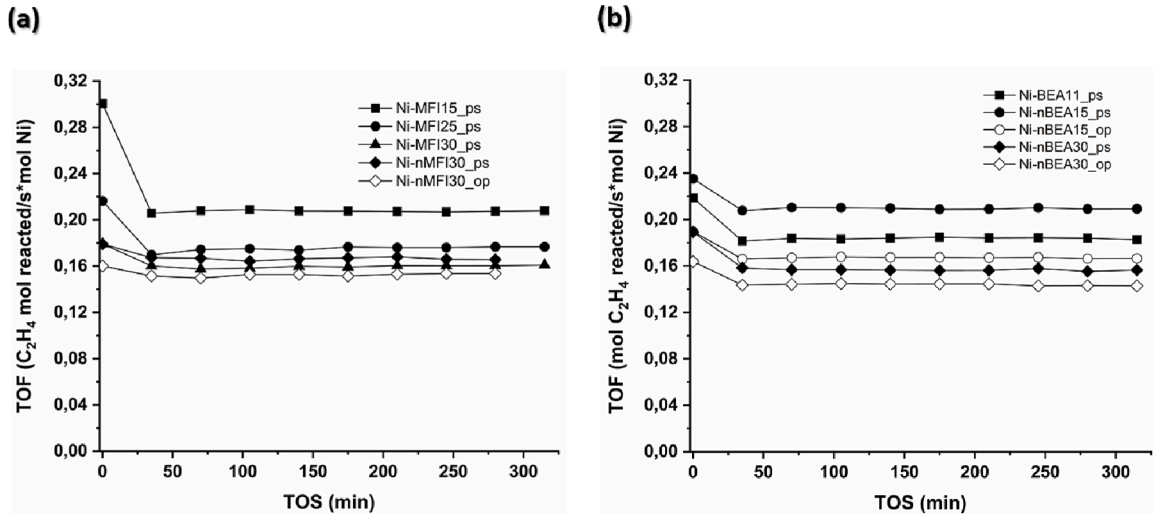

Fig. 6. Reacted ethylene (mol) normalized by Ni content in Ni-containing MFI (a) and BEA (b) materials under near-ambient pressure. Reaction conditions: 180 °C, 2.5 bar, WHSV = 16.3 hr^{-1}, Q_t = 600 mL/min (%vol N_2 = 97.5, %vol C_2H_4 = 2.5%), m_{cat} = 63 mg.

to the formation of long chain alkyl-nickel attachments by the effect of Brønsted acid sites in close proximity within the zeolite pores, resulting in the partial blocking of the Ni^{2+} active sites.[21] A similar deactivation behaviour was described in a recent study by Moussa et al.,[26] were the activity loss was related to the irreversible adsorption of reaction intermediates on cationic Ni^{2+} species in ion-exchange positions, with strong Lewis acidity. For the Ni-MFI samples, increasing Si/Al leads to a decrease in the TOF, not only initially (TOS = 0 min) but also at longer times. At his point it is important to remark that, according to the literature,[55–60] Ni^{2+} species are the most active for the activation of the ethylene molecule and that Ni-free acid zeolites present no ethylene conversion under our experimental conditions (results not shown). Thus, the activity trends observed for the Ni-MFI with different Al content will be related to the ability of the MFI supports for stabilizing these cationic Ni species. Indeed, the FTIR-pyridine results evidenced that the highest loss of Brønsted acid site density and the highest increase in the number of Lewis acid sites were observed for the most active sample, Ni-MFI15_ps, which also presented the largest proportion of cationic Ni^{2+} in charge-compensation sites according to the low temperature CO adsorption results. Lower Al contents and smaller crystal size led to an increase of Si-OH grafted Ni^{2+} species, with milder Lewis acidity, which have been described as active for the ethylene oligomerization reaction,[21] especially at longer TOS.[26] This would also explain the lower deactivation rate, as lower interaction of these weaker Lewis acid sites with adsorbed species will reduce irreversible site blockage.[26,45] Regarding the influence of the crystal size in these Ni-ZSM-5, the same initial activity is obtained for the nanocrystalline Ni-nMFI30_ps and the commercial-based Ni-MFI30_ps, but the former presents a lower deactivation rate as could be expected from the shorter diffusional paths (see Table S2). Finally, the Ni-ZSM-5 prepared by one-pot synthesis, Ni-nMFI30_op, with the lowest proportion of ion-exchanged Ni^{2+} and a significant amount of NiO nanoparticles, is the less active sample as compared to the catalysts obtained by post-synthesis Ni impregnation.

Similar trends are observed for the Beta-based catalysts (see Fig. 6b). Comparing the two non-commercial nano-crystalline Ni-containing zeolites, higher Al content (Si/Al = 15) and Ni incorporation by post-synthesis impregnation leads to more active catalysts than their counterparts with higher Si/Al = 30 and/or prepared by direct synthesis. Again, this can be related to a better stabilization of ion-exchanged Ni^{2+} species for higher Al contents and a lower tendency to the formation of NiO nanoparticles when introducing the metal by post-synthesis methods, respectively. Catalyst Ni-BEA11_ps, based on the commercial nanosized Beta, presents an intermediate activity as compared to Ni-nBEA15_ps and Ni-nBEA30_ps and a stronger deactivation during the first stages of the reaction. This could be explained by its larger crystallite dimensions, a behaviour that has also been observed in the oligomerization of larger olefins.[16].

According to the product distribution obtained with the MFI-based catalysts (see Fig. 7a, 7b and S10), the main products observed after two hours on stream are in all cases the butenes obtained by dimerization, with selectivities above 75%. However, during the first stages of

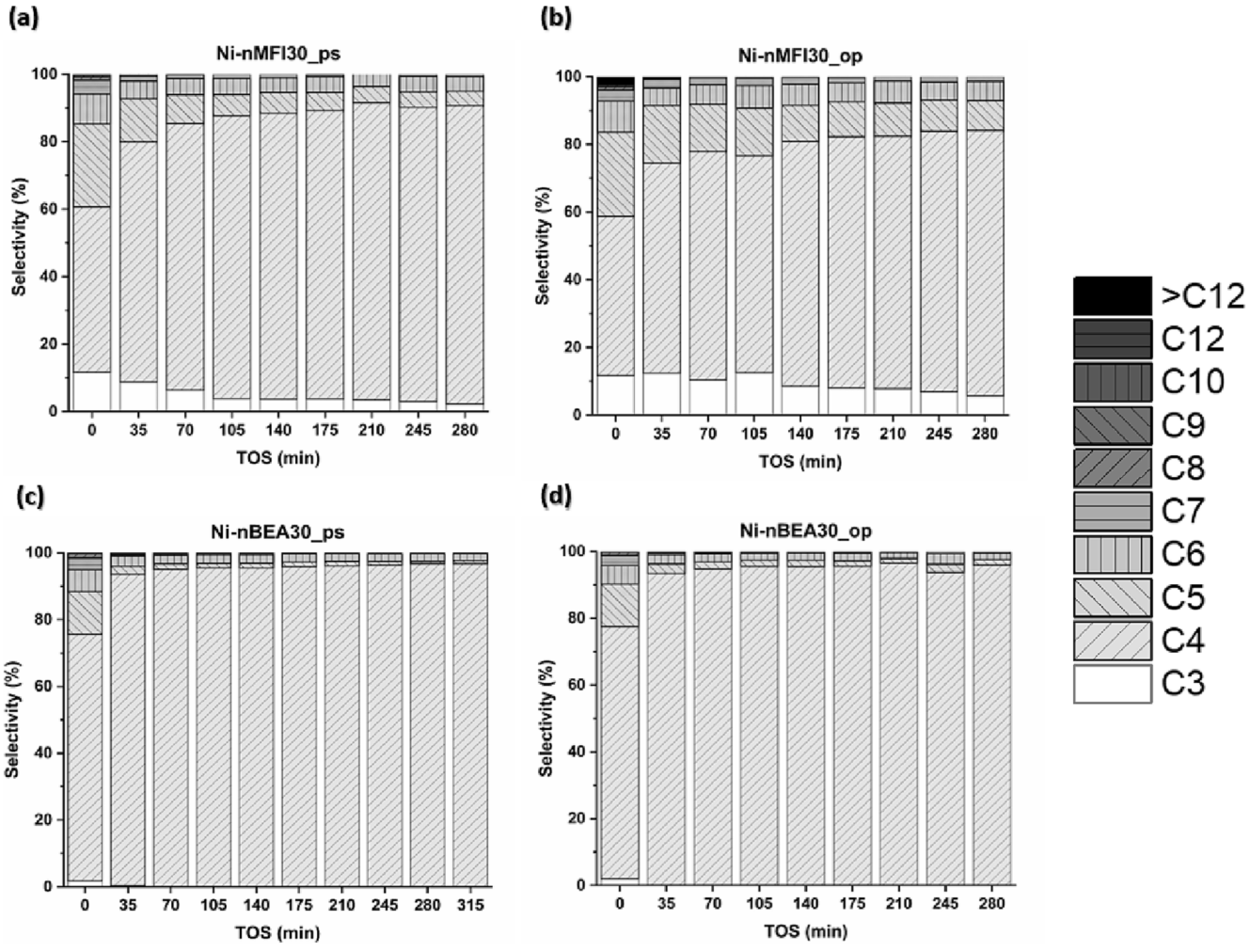

Fig. 7. Product selectivities for Ni-containing nanosized MFI (a,b) and nanosized BEA (c,d) materials under near-ambient pressure. Reaction conditions: 180 °C, 2.5 bar, WHSV = 16.3 hr^{-1}, Q_t = 600 mL/min (%vol N_2 = 97.5, %vol C_2H_4 = 2.5%), m_{cat} = 63 mg.

the reaction, when the activity of the catalysts is higher, additional products are observed, mainly C_3, C_5, C_6 and C_7. The presence of olefins with odd number of carbons indicate that, besides true oligomerization of ethylene occurring on the active Ni sites, other side reactions such as oligomerization of primary products, isomerization and cracking are taking place on the Brønsted acid sites.[61] The formation of small amounts of isobutane during these initial stages of the reaction (results not shown) supports the contribution of these carbocation-based mechanisms to the overall product distribution observed. The strong deactivation observed during the first hour of reaction, the stabilization of ethylene conversion at longer TOS and the evolution of the product distribution with time, suggest that the Brønsted acid sites, responsible for the oligomerization-cracking, deactivate faster than the active Ni species. The lowest selectivity to butenes and highest selectivity to C_3 and C_{5+} products is obtained with catalyst Ni-nMFI30_op, despite its lower activity as compared to the rest of the Ni-MFI catalysts. This could be related to the larger Brønsted acid site density of this sample prepared by one-pot synthesis (see Table 4).

Regarding the product selectivities obtained with the Beta-based catalysts (see Fig. 7c, 7d and S11), butenes were the main products also in this case. However, the selectivity to these dimers was higher than for the ZSM-5-based catalysts, with values above 90% under steady-state conditions in most of the cases. Only at very short TOS (<36 min) some C_3 and significant amounts of C_5, C_6 and C_7 hydrocarbons were observed, produced by isomerization-cracking of heavier oligomers, probably at the channel intersections.[61] Isobutane is also formed at short TOS in this case (results not shown), but in larger amounts than for ZSM-5 due to the larger hydrogen transfer capacity of the large pore Beta zeolite.

Based on the catalytic results obtained under near ambient pressure conditions, high space velocities and low ethylene partial pressure, it can be concluded that the catalysts with post-synthetic Ni incorporation show better catalytic performance than those prepared by one-pot methods. The post-synthetic incorporation of Ni maximizes the stabilization of cationic Ni^{2+} species, particularly in those samples with lower Si/Al molar ratios, as evidenced in the former section by the combination of different characterization techniques (i.e. “in-situ” IR experiments with probe molecules and H_2-TPR).

When the ethylene oligomerization reaction was performed at higher total and ethylene partial pressure, higher temperature and lower space velocity, important and interesting differences are observed for the catalysts compared. Under these conditions, more representative of industrial operation, the TOF values (see Fig. 8) obtained with the Ni-containing zeolites are lower than those obtained under near-ambient pressure (see Fig. 6) due to the higher ethylene/Ni ratios employed in this second approach, in good agreement with previous works.[26] Moreover, the higher pressure and ethylene concentration in the feed will also result in the formation of larger oligomers, as will be shown later, leading to a faster catalyst deactivation. Thus, other factors, besides Ni speciation, are expected to play an important role in the catalytic behaviour, such as the crystal size of the zeolites and the remaining Brønsted acidity of the bifuncional Ni-catalysts.

This is, indeed, what can be deduced from the activity curves (see Fig. 8) and from the values enclosed in Table S2. According to the results obtained with the MFI-based samples under near-ambient pressure conditions, the initial activity and the deactivation rate increased with the Si/Al ratio, e.g., with the proportion of Ni^{2+} in ion exchange positions, and crystal size did not have a major influence. However, under high pressure and high ethylene concentration in the feed, the most active Ni-MFIs are the two nanocrystalline zeolites, which also present the best stability with TOS. Moreover, nickel incorporation does not seem to affect significantly the activity of the catalysts. Thus, whereas for low pressure, low partial pressures and high WHSV, ethylene activation on the different Ni species was playing a main role in the conversion of the olefin, under industrially relevant conditions the activity and deactivation rates are dominated by the zeolite crystal size.

In case of the Ni-BEA catalysts, all of them with nano-sized crystallites in the range of 10–30 nm, the differences in initial activity are smaller. Still, higher Al contents and better stabilization of cationic Ni^{2+} in charge compensating sites result in higher ethylene conversions and lower deactivation degrees (see Fig. 8b and Table S2).

The product distribution obtained for the Ni-containing MFI and BEA catalysts are compared in Figs. 9, S12 and S13. The first thing to be noted is that the product distribution is significantly different than the one obtained under conditions of lower pressure and ethylene partial pressure. Moreover, both the crystal size and the Ni incorporation method are affecting in a much higher degree the final product selectivity within the hydrocarbons. Thus, the commercial MFI-based catalysts present a product distribution more similar to the one obtained under lower pressure conditions, with C_5^+ oligomers formed on the fresh catalyst at short TOS, and butenes' selectivity above 70% for longer times (see Figure S12). However, under these high-pressure conditions, consecutive ethylene oligomerization steps will be more favored and the extension of cracking reactions will be reduced,[62] leading to higher selectivity to trimers and tetramers (C_6 and C_8) and decreasing the production of C_5 hydrocarbons (see Figure S12). In fact, the selectivity to C_3 hydrocarbons is lower under these conditions, suggesting their participation in the formation of larger oligomers. On the other hand,

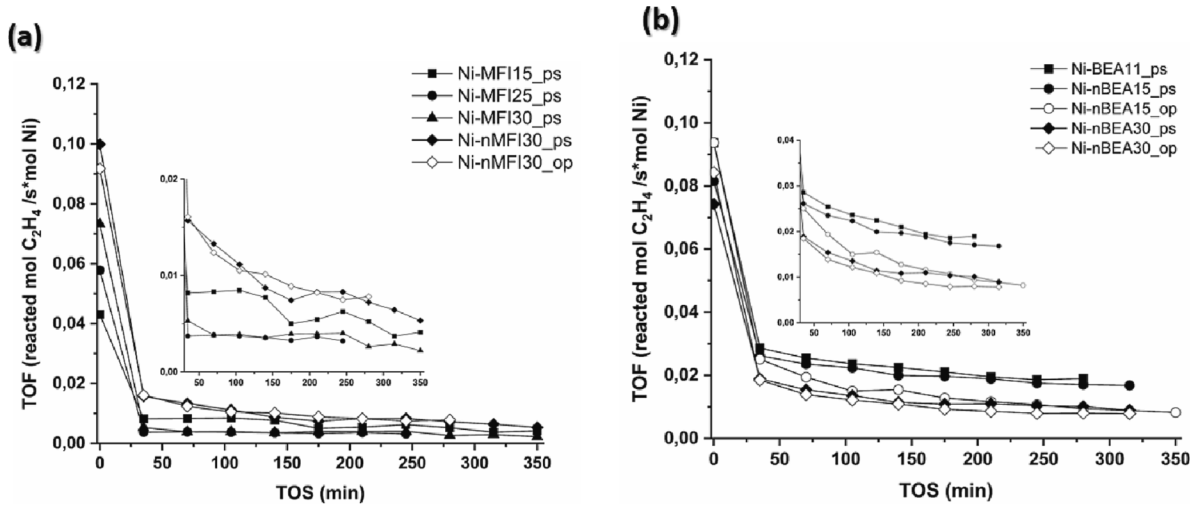

Fig. 8. Reacted ethylene (mol) normalized by Ni content in Ni-containing MFI (a) and BEA (b) materials under high-pressure conditions. Reaction conditions: 200 °C, 35 bar, WHSV = 2.1 hr^{-1}, Q_t = 100 mL/min (%vol N_2 = 85, %vol C_2H_4 = 15%), m_{cat} = 500 mg.

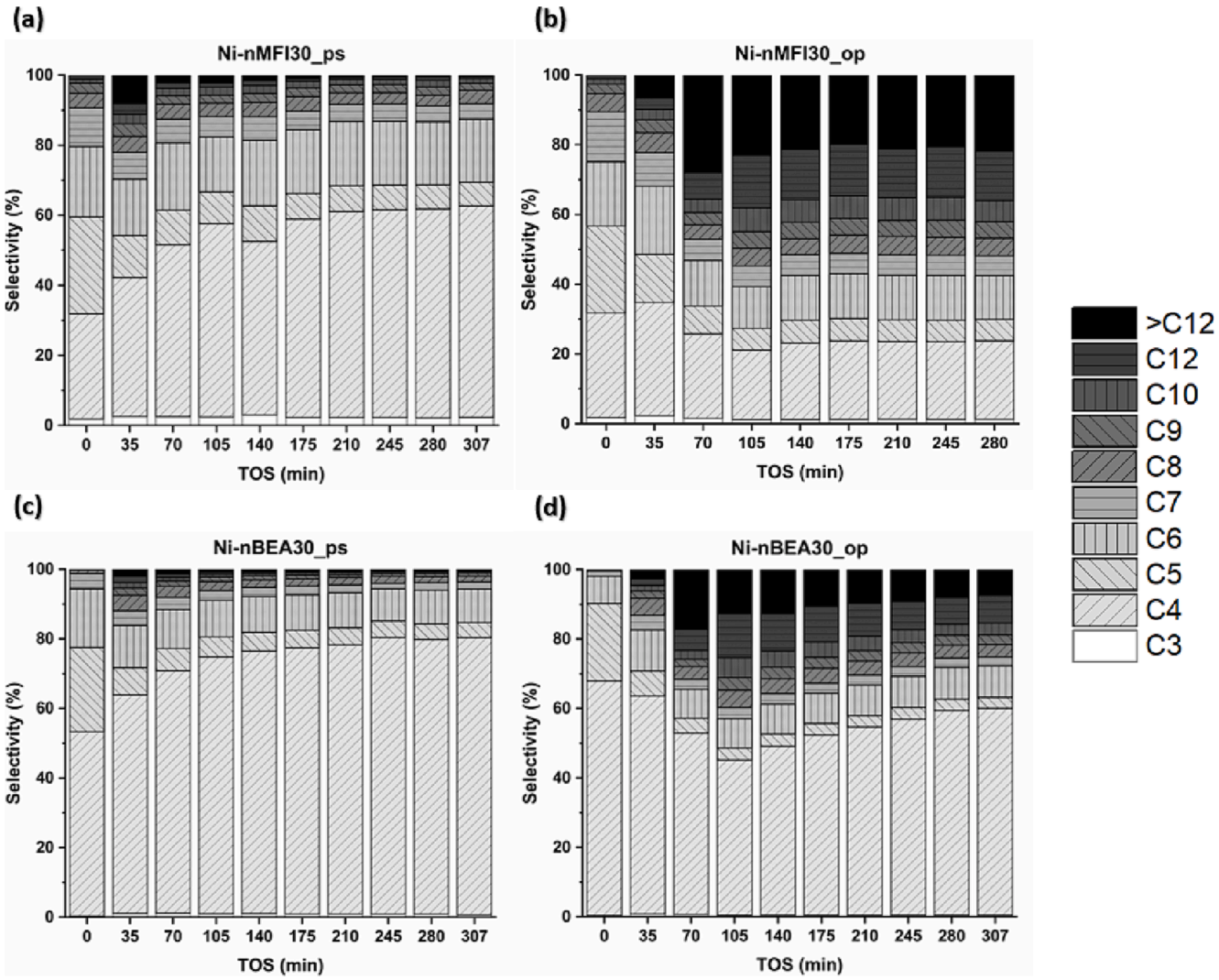

Fig. 9. Product selectivities for Ni-containing nanosized MFI (a,b) and nanosized BEA (c,d) materials under high-pressure conditions. Reaction conditions: 200 °C, 35 bar, WHSV = 2.1 hr^{-1}, Q_t = 100 mL/min (%vol N_2 = 85, %vol C_2H_4 = 15%), m_{cat} = 500 mg.

the nano-ZSM-5 are much more selective to C_5^+ products than the micron-sized catalysts with comparable Si/Al ratio thanks to their shorter diffusional path lengths that will facilitate the elution of the heavier oligomers out of the zeolite crystals (see Fig. 9). Moreover, catalysts Ni-nMFI30_op obtained by direct synthesis metal incorporation, with higher Brønsted acid site density as compared to Ni-nMFI30_ps, will increase even more the number of oligomerization steps leading to the formation of important amounts of C_{12}^+ products (see Fig. 9b).

The differences in product selectivity are even larger when comparing the results obtained with the Ni-Beta-based catalysts under the two reaction conditions. These samples, highly selective to butenes under near-ambient pressure (>90% for TOS $\geq$ 36 min), also favor the formation of heavier products under conditions of higher total pressure, mainly of oligomers with even carbon numbers (see Fig. 9c, 9d and S13). As in the case of the MFI-based samples, the higher Brønsted acid site density of the catalysts prepared by Ni incorporation by direct one-pot synthesis (see Table 4) leads to an increase in the number of oligomerization steps, increasing the proportion of C_{12} and C_{12}^+ hydrocarbons as compared to the Ni-nBEAs obtained by post-synthesis Ni impregnation (see Fig. 9d and S13b). Thus, under these conditions of higher total pressure, higher ethylene concentration and lower space velocity, the catalytic behavior of the Ni-zeolites compared in this work is more dependent on the crystal size and on the number of Brønsted acid sites than on the Ni speciation. Under these higher total and ethylene partial pressure conditions bimolecular reactions such as hydrogen transfer are more favored as compared to near-ambient, low alkene partial pressure, and the proportion of isobutane at short TOS is higher in the former case. However, under both conditions, MFI is less selective to isobutane than Beta, Ni-nBEA obtained by one-pot synthesis are more selective than the catalysts prepared by post-synthesis impregnation, in good agreement with their larger density of Brønsted acid sites, and after 1 h on stream the selectivity to isobutane is in all cases below 5% (results not shown).

From the catalytic study, it can be concluded that the rationalized synthesis of Ni-containing zeolites controlling the zeolite topology and crystal size, the Ni speciation and the acidic properties of the support, allows improving initial activity and catalyst life and increasing the selectivity towards liquid fuels (C_5^+ hydrocarbons) when working under industrially relevant conditions. We have shown that although crystal size has only a minor influence when ethylene is converted under conditions involving a reduced number of oligomerization steps (low total and ethylene partial pressure, high space velocity) it plays a crucial role when moving into higher pressures and higher ethylene/catalyst ratios. Regarding the nanosized MFI- and BEA-based catalysts, we have seen that the type of Ni species formed is highly dependent on the metal incorporation method for both zeolites structures and for two Si/Al ratios in case of BEA. Higher activity is obtained, independently of the experimental conditions employed for ethylene conversion, when Ni is

added by post-synthesis impregnation due to a larger amount of Ni^{2+} species present in these samples. As this has a direct influence on the number of Brønsted acid sites remaining on the final bifunctional catalyst, the Ni incorporation procedure will also determine the final product distribution and deactivation rate, especially under high-pressure conditions where the formation of C_5^+ hydrocarbons is favored.

4. Conclusions

A set of Ni-containing zeolites has been prepared varying the crystalline structure, the crystal sizes, the Si/Al ratio and the Ni incorporation method. By means of complementary characterization techniques it has been determined that Nickel incorporation by post-synthesis impregnation leads to higher contents of cationic Ni^{2+} in ion exchange positions, and that the stabilization of these species is favoured for zeolites with higher Al contents (lower Si/Al ratios), whereas the one-pot synthesis of nanocrystalline Ni-zeolites favours the formation of NiO nanoclusters inside the zeolitic pores.

The catalytic behaviour of these samples for the conversion of ethylene has been compared under two sets of reaction conditions, under near ambient pressure, low partial pressure and high space velocity, on the one hand, and working at higher total pressure, lower space velocity and higher ethylene concentration in the feed, on the other. Under the conditions employed in the first approach, crystal size does not play a decisive role and the catalysts with post-synthetic Ni incorporation show better catalytic performance than those prepared by one-pot methods. The post-synthetic incorporation of Ni maximizes the stabilization of Ni^{2+} species, particularly in those samples with lower Si/Al molar ratios, species that are known to be the most active for ethylene activation and dimerization. However, when working under higher pressures and higher ethylene/catalyst ratios, conditions that favour a larger number of oligomerization steps and the formation of heavier hydrocarbons, the crystal size plays a crucial role, and the nano-sized zeolites are more active and more stable towards deactivation than the commercial-based catalysts with larger crystals. Comparing the nanocrystalline catalysts prepared by means of different Ni incorporation methods, also in this case the activity obtained is higher with the catalysts in which Ni is added by post-synthesis impregnation. Moreover, as this has a direct influence on the number of Brønsted acid sites remaining on the final bifunctional catalyst, the Ni incorporation procedure also has an important influence in the final product distribution obtained under these high-pressure conditions.

Declaration of Competing Interest

The authors declare that they have no known competing financial interests or personal relationships that could have appeared to influence the work reported in this paper.

Data availability

Data will be made available on request.

Acknowledgements

This work has been supported by Spanish Government through PID2021-122755OB-I00 funded by MCIN/AEI/10.13039/501100011033 and TED2021-130739B–I00 funded by MCIN/AEI/10.13039/501100011033/EU/PRTR), and by Generalitat Valenciana through AICO/2021/201. Financial support by Severo Ochoa centre of excellence program (CEX2021-001230-S) is also gratefully acknowledged. AMGA acknowledges the Spanish Government for a Severo Ochoa FPI scholarship (PRE2019-088361). J. M. Salas is acknowledged for his contribution to CO-IR experiments. The Electron Microscopy Service of the UPV is also acknowledged for their help in sample characterization.

Appendix A. Supplementary material

Supplementary data to this article can be found online at https://doi.org/10.1016/j.jcat.2023.07.010.

References:

[1] A. Boulamanti, J.A. Moya, Production costs of the chemical industry in the EU and other countries: Ammonia, methanol and light olefins, Renew. Sustain. Energy Rev. 68 (2017) 1205–1212, https://doi.org/10.1016/j.rser.2016.02.021.
[2] Z. Zhao, J. Jiang, F. Wang, An economic analysis of twenty light olefin production pathways, J. Energy Chem. 56 (2021) 193–202, https://doi.org/10.1016/j.jechem.2020.04.021.
[3] P. Tian, Y. Wei, M. Ye, Z. Liu, Methanol to Olefins (MTO): From Fundamentals to Commercialization, ACS Catal. 5 (2015) 1922–1938, https://doi.org/10.1021/acscatal.5b00007.
[4] P.S. Rezaei, H. Shafaghat, W.M.A.W. Daud, Production of green aromatics and olefins by catalytic cracking of oxygenate compounds derived from biomass pyrolysis: A review, Appl. Catal. A Gen. 469 (2014) 490–511, https://doi.org/10.1016/j.apcata.2013.09.036.
[5] P. Gao, S. Dang, S. Li, X. Bu, Z. Liu, M. Qiu, C. Yang, H. Wang, L. Zhong, Y. Han, Q. Liu, W. Wei, Y. Sun, Direct Production of Lower Olefins from CO2 Conversion via Bifunctional Catalysis, ACS Catal. 8 (2018) 571–578, https://doi.org/10.1021/acscatal.7b02649.
[6] A. Corma, S. Iborra, Oligomerization of Alkenes, in: Catal. Fine Chem. Synth., John Wiley & Sons, Ltd, Chichester, UK, 2006: pp. 125–140. 10.1002/0470094214.ch6.
[7] W. Vermeiren, J.-P. Gilson, Impact of Zeolites on the Petroleum and Petrochemical Industry, Top. Catal. 52 (2009) 1131–1161, https://doi.org/10.1007/s11244-009-9271-8.
[8] C. Martínez, A. Corma, Inorganic molecular sieves: Preparation, modification and industrial application in catalytic processes, Coord. Chem. Rev. 255 (2011) 1558–1580, https://doi.org/10.1016/j.ccr.2011.03.014.
[9] C.P. Nicholas, Applications of light olefin oligomerization to the production of fuels and chemicals, Appl. Catal. A Gen. 543 (2017) 82–97, https://doi.org/10.1016/j.apcata.2017.06.011.
[10] G. Bellussi, F. Mizia, V. Calemma, P. Pollesel, R. Millini, Oligomerization of olefins from Light Cracking Naphtha over zeolite-based catalyst for the production of high quality diesel fuel, Microporous Mesoporous Mater. 164 (2012) 127–134, https://doi.org/10.1016/j.micromeso.2012.07.020.
[11] J.A. Martens, R. Ravishankar, I.E. Mishin, P.A. Jacobs, Tailored Alkene Oligomerization with H-ZSM-57 Zeolite, Angew, Chemie. 39 (2000) 4376–4379, https://doi.org/10.1002/1521-3773(20001201)39:23<4376::AID-ANIE4376>3.0.CO;2-2.
[12] A.N. Mlinar, P.M. Zimmerman, F.E. Celik, M. Head-Gordon, A.T. Bell, Effects of Brønsted-acid site proximity on the oligomerization of propene in H-MFI, J. Catal. 288 (2012) 65–73, https://doi.org/10.1016/j.jcat.2012.01.002.
[13] A. Corma, C. Martínez, E. Doskocil, Designing MFI-based catalysts with improved catalyst life for oligomerization to high-quality liquid fuels, J. Catal. 300 (2013) 183–196, https://doi.org/10.1016/j.jcat.2012.12.029.
[14] J.P.G. Pater, P.A. Jacobs, J.A. Martens, 1-Hexene Oligomerization in Liquid, Vapor, and Supercritical Phases over Beidellite and Ultrastable Y Zeolite Catalysts, J. Catal. 179 (1998) 477–482, https://doi.org/10.1006/jcat.1998.2250.
[15] R. Martínez-Franco, C. Paris, M.E. Martínez-Armero, C. Martínez, M. Moliner, A. Corma, High-silica nanocrystalline Beta zeolites: efficient synthesis and catalytic application, Chem. Sci. 7 (2016) 102–108, https://doi.org/10.1039/C5SC03019F.
[16] M.R. Díaz-Rey, C. Paris, R. Martínez-Franco, M. Moliner, C. Martínez, A. Corma, Efficient Oligomerization of Pentene into Liquid Fuels on Nanocrystalline Beta Zeolites, ACS Catal. 7 (2017) 6170–6178, https://doi.org/10.1021/acscatal.7b00817.
[17] H. Olivier-Bourbigou, P.A.R. Breuil, L. Magna, T. Michel, M.F. Espada Pastor, D. Delcroix, Nickel Catalyzed Olefin Oligomerization and Dimerization, Chem. Rev. 120 (2020) 7919–7983, https://doi.org/10.1021/acs.chemrev.0c00076.
[18] J. Heveling, A. van der Beek, M. de Pender, Oligomerization of ethene over nickel-exchanged zeolite y into a diesel-range product, Appl. Catal. 42 (1988) 325–336, https://doi.org/10.1016/0166-9834(88)80011-3.
[19] F.T.T. Ng, D.C. Creaser, Ethylene dimerization over modified nickel exchanged Y-zeolite, Appl. Catal. A Gen. 119 (1994) 327–339, https://doi.org/10.1016/0926-860X(94)85200-6.
[20] B. Nkosi, F.T.T. Ng, G.L. Rempel, The oligomerization of butenes with partially alkali exchanged NiNaY zeolite catalysts, Appl. Catal. A Gen. 158 (1997) 225–241, https://doi.org/10.1016/S0926-860X(96)00420-6.
[21] S. Moussa, P. Concepción, M.A. Arribas, A. Martínez, The nature of active Ni sites and the role of Al species in the oligomerization of ethylene on mesoporous Ni-Al-MCM-41 catalysts, Appl. Catal. A Gen. 608 (2020), 117831, https://doi.org/10.1016/j.apcata.2020.117831.
[22] M. Lallemand, A. Finiels, F. Fajula, V. Hulea, Nature of the Active Sites in Ethylene Oligomerization Catalyzed by Ni-Containing Molecular Sieves: Chemical and IR Spectral Investigation, J. Phys. Chem. C. 113 (2009) 20360–20364, https://doi.org/10.1021/jp9082932.
[23] F. Jin, Y. Yan, G. Wu, Ethylene oligomerization over H- and Ni-form aluminosilicate composite with ZSM-5 and MCM-41 structure: Effect of acidity strength, nickel site and porosity, Catal. Today. 355 (2020) 148–161, https://doi.org/10.1016/j.cattod.2019.06.050.

[24] E. Koninckx, P.S.F. Mendes, J.W. Thybaut, L.J. Broadbelt, Ethylene oligomerization on nickel catalysts on a solid acid support: From New mechanistic insights to tunable bifunctionality, Appl. Catal. A Gen. 624 (2021), 118296, https://doi.org/10.1016/j.apcata.2021.118296.
[25] A. Ehrmaier, S. Peitz, M. Sanchez-Sanchez, R. Bermejo-Deval, J. Lercher, On the role of co-cations in nickel exchanged LTA zeolite for butene dimerization, Microporous Mesoporous Mater. 284 (2019) 241–246, https://doi.org/10.1016/j.micromeso.2019.03.047.
[26] S. Moussa, P. Concepción, M.A. Arribas, A. Martínez, Nature of Active Nickel Sites and Initiation Mechanism for Ethylene Oligomerization on Heterogeneous Ni-beta Catalysts, ACS Catal. 8 (2018) 3903–3912, https://doi.org/10.1021/acscatal.7b03970.
[27] A. Brückner, U. Bentrup, H. Zanthoff, D. Maschmeyer, The role of different Ni sites in supported nickel catalysts for butene dimerization under industry-like conditions, J. Catal. 266 (2009) 120–128, https://doi.org/10.1016/j.jcat.2009.05.021.
[28] T. Yashima, Y. Ushida, M. Ebisawa, N. Hara, Polymerization of ethylene over transition-metal exchanged Y zeolites, J. Catal. 36 (1975) 320–326, https://doi.org/10.1016/0021-9517(75)90042-1.
[29] M.D. Leatherman, M. Brookhart, Ni(II)-Catalyzed Polymerization of trans -2-Butene, Macromolecules 34 (2001) 2748–2750, https://doi.org/10.1021/ma002142j.
[30] H. Choo, S.B. Hong, L. Kevan, Comparative ESR Studies on the Reducibility and Adsorbate Interactions of Paramagnetic Ni(I) in Synthetic Ferrierite and Mordenite, J. Phys. Chem. B. 105 (2001) 1995–2002, https://doi.org/10.1021/jp0036341.
[31] R.Y. Brogaard, U. Olsbye, Ethene Oligomerization in Ni-Containing Zeolites: Theoretical Discrimination of Reaction Mechanisms, ACS Catal. 6 (2016) 1205–1214, https://doi.org/10.1021/acscatal.5b01957.
[32] A. Saxena, R. Joshi, R.R. Seemakurthi, E. Koninckx, L.J. Broadbelt, J. Greeley, R. Gounder, Effect of Nickel Active Site Density on the Deactivation of Ni-Beta Zeolite Catalysts during Ethene Dimerization, ACS Eng. Au. 2 (2022) 12–16, https://doi.org/10.1021/acsengineeringau.1c00014.
[33] A. Martínez, M.A. Arribas, P. Concepción, S. Moussa, New bifunctional Ni–H-Beta catalysts for the heterogeneous oligomerization of ethylene, Appl. Catal. A Gen. 467 (2013) 509–518, https://doi.org/10.1016/j.apcata.2013.08.021.
[34] R. Zăvoianu, C. Nenu, E. Angelescu, Ni(2,2′-bipyridine)2Cl2 encapsulated in Y zeolite new catalyst for ethylene dimerization, Catal. Commun. 6 (2005) 415–420, https://doi.org/10.1016/j.catcom.2005.03.007.
[35] M.L. Mignoni, M.O. de Souza, S.B.C. Pergher, R.F. de Souza, K. Bernardo-Gusmão, Nickel oligomerization catalysts heterogenized on zeolites obtained using ionic liquids as templates, Appl. Catal. A Gen. 374 (2010) 26–30, https://doi.org/10.1016/j.apcata.2009.11.017.
[36] Y. Yang, Y. Lyu, L. Zhao, W. Zhan, L. Fan, F. Li, X. Liu, Ligand assistance via solid-state coordination for promoting nickel dispersion over the Ni/Beta hydroisomerization catalyst, Fuel 318 (2022), 123568, https://doi.org/10.1016/j.fuel.2022.123568.
[37] B.P. Nicola, C.W. Lopes, C. Marini, E. Rossetto, S.B.C. Pergher, K. Bernardo-Gusmão, Ni-β-diimine complex heterogenized in delaminated ITQ-2 zeolite as catalytic precursor for ethylene oligomerization, Catal. Today. 381 (2021) 192–199, https://doi.org/10.1016/j.cattod.2020.07.019.
[38] Q. Sun, N. Wang, J. Yu, Advances in Catalytic Applications of Zeolite-Supported Metal Catalysts, Adv. Mater. 33 (2021) 2104442, https://doi.org/10.1002/adma.202104442.
[39] L. Liu, A. Corma, Confining isolated atoms and clusters in crystalline porous materials for catalysis, Nat. Rev. Mater. 6 (2021) 244–263, https://doi.org/10.1038/s41578-020-00250-3.
[40] S. Moon, H.-J. Chae, M.B. Park, Oligomerization of light olefins over ZSM-5 and beta zeolite catalysts by modifying textural properties, Appl. Catal. A Gen. 553 (2018) 15–23, https://doi.org/10.1016/j.apcata.2018.01.015.
[41] E.M. Gallego, C. Paris, M.R. Díaz-Rey, M.E. Martínez-Armero, J. Martínez-Triguero, C. Martínez, M. Moliner, A. Corma, Simple organic structure directing agents for synthesizing nanocrystalline zeolites, Chem. Sci. 8 (2017) 8138–8149, https://doi.org/10.1039/C7SC02858J.
[42] C.A. Emeis, Determination of Integrated Molar Extinction Coefficients for Infrared Absorption Bands of Pyridine Adsorbed on Solid Acid Catalysts, J. Catal. 141 (1993) 347–354, https://doi.org/10.1006/jcat.1993.1145.
[43] M.I. Vázquez, A. Corma, V. Fornés, Characterization of NiO supported on zeolite Y, by pyridine adsorption, Zeolites 6 (1986) 271–274, https://doi.org/10.1016/0144-2449(86)90080-1.
[44] Y. Ganjkhanlou, E. Groppo, S. Bordiga, M.A. Volkova, G. Berlier, Incorporation of Ni into HZSM-5 zeolites: Effects of zeolite morphology and incorporation procedure, Microporous Mesoporous Mater. 229 (2016) 76–82, https://doi.org/10.1016/j.micromeso.2016.04.002.
[45] S. Moussa, M.A. Arribas, P. Concepción, A. Martínez, Heterogeneous oligomerization of ethylene to liquids on bifunctional Ni-based catalysts: The influence of support properties on nickel speciation and catalytic performance, Catal. Today. 277 (2016) 78–88, https://doi.org/10.1016/j.cattod.2015.11.032.
[46] K. Hadjiivanov, H. Knözinger, M. Mihaylov, FTIR Study of CO Adsorption on Ni−ZSM-5, J. Phys. Chem. B. 106 (2002) 2618–2624, https://doi.org/10.1021/jp0132782.
[47] P. Pietrzyk, K. Podolska, Z. Sojka, Role of NO δ+ Intermediates in NO Reduction with Propene over NiZSM-5 Zeolite Revealed by EPR and IR Spectroscopic Investigations and DFT Modeling, J. Phys. Chem. C. 115 (2011) 13008–13015, https://doi.org/10.1021/jp203188k.
[48] A. Penkova, S. Dzwigaj, R. Kefirov, K. Hadjiivanov, M. Che, Effect of the Preparation Method on the State of Nickel Ions in BEA Zeolites. A Study by Fourier Transform Infrared Spectroscopy of Adsorbed CO and NO, Temperature-Programmed Reduction, and X-Ray Diffraction, J. Phys. Chem. C. 111 (2007) 8623–8631, https://doi.org/10.1021/jp071927p.
[49] H.A. Aleksandrov, V.R. Zdravkova, M.Y. Mihaylov, P. St, G.N. Petkov, K.I. H. Vayssilov, Precise Identification of the Infrared Bands of the Polycarbonyl Complexes on Ni–MOR Zeolite by 12C16O–13C18O Coadsorption and Computational Modeling, J. Phys. Chem. C. 116 (2012) 22823–22831, https://doi.org/10.1021/jp304972u.
[50] A. Zecchina, S. Bordiga, G. Spoto, L. Marchese, G. Petrini, G. Leofanti, M. Padovan, Silicalite characterization. 1. Structure, adsorptive capacity, and IR spectroscopy of the framework and hydroxyl modes, J. Phys. Chem. 96 (1992) 4985–4990, https://doi.org/10.1021/j100191a047.
[51] I. Braschi, G. Gatti, C. Bisio, G. Berlier, V. Sacchetto, M. Cossi, L. Marchese, The Role of Silanols in the Interactions between Methyl tert -Butyl Ether and High-Silica Faujasite Y: An Infrared Spectroscopy and Computational Model Study, J. Phys. Chem. C. 116 (2012) 6943–6952, https://doi.org/10.1021/jp210605t.
[52] R. Baran, A. Śrębowata, I.I. Kamińska, D. Łomot, S. Dzwigaj, Catalytic activity of HAlBEA and NixHAlBEA zeolites in hydrogen-assisted dehydrochlorination of 1,2-dichloroethane into vinyl chloride monomer, Microporous Mesoporous Mater. 180 (2013) 209–218, https://doi.org/10.1016/j.micromeso.2013.06.037.
[53] A.N. Mlinar, G.B. Baur, G.G. Bong, A.“. Getsoian, A.T. Bell, “Bean” Getsoian, A.T. Bell, Propene oligomerization over Ni-exchanged Na-X zeolites, J. Catal. 296 (2012) 156–164.
[54] L. Wang, T. Chen, J. Zhang, Y. Jiao, J. Wang, Q. Zhu, X. Li, High catalytic activity and stability quasi homogeneous alkali metal promoted Ni/SiO2 aerogel catalysts for catalytic cracking of n-decane, Fuel 268 (2020), 117384, https://doi.org/10.1016/j.fuel.2020.117384.
[55] A. Ehrmaier, Y. Liu, S. Peitz, A. Jentys, Y.-H.-C. Chin, M. Sanchez-Sanchez, R. Bermejo-Deval, J. Lercher, Dimerization of Linear Butenes on Zeolite-Supported Ni2+, ACS Catal. 9 (2019) 315–324, https://doi.org/10.1021/acscatal.8b03095.
[56] M. Meloni, R.C. Runnebaum, Tuning supported Ni catalysts by varying zeolite Beta heteroatom composition: effects on ethylene adsorption and dimerization catalysis, Catal. Sci. Technol. 11 (2021) 3393–3401, https://doi.org/10.1039/D1CY00308A.
[57] W. Li, C. Zhou, W. Li, L. Ge, G. Yu, M. Qiu, X. Chen, Tuning the Ni site location of bifunctional Ni-based catalysts for improving the performance in ethylene oligomerization, New J. Chem. 46 (2022) 9461–9469, https://doi.org/10.1039/D2NJ01527G.
[58] R. Henry, M. Komurcu, Y. Ganjkhanlou, R.Y. Brogaard, L. Lu, K.-J. Jens, G. Berlier, U. Olsbye, Ethene oligomerization on nickel microporous and mesoporous-supported catalysts: Investigation of the active sites, Catal. Today. 299 (2018) 154–163, https://doi.org/10.1016/j.cattod.2017.04.029.
[59] A. Lacarriere, J. Robin, D. Świerczyński, A. Finiels, F. Fajula, F. Luck, V. Hulea, Distillate-Range Products from Non-Oil-Based Sources by Catalytic Cascade Reactions, ChemSusChem 5 (2012) 1787–1792, https://doi.org/10.1002/cssc.201200092.
[60] R. Joshi, G. Zhang, J.T. Miller, R. Gounder, Evidence for the Coordination-Insertion Mechanism of Ethene Dimerization at Nickel Cations Exchanged onto Beta Molecular Sieves, ACS Catal. 8 (2018) 11407–11422, https://doi.org/10.1021/acscatal.8b03202.
[61] M.L. Sarazen, E. Doskocil, E. Iglesia, Effects of Void Environment and Acid Strength on Alkene Oligomerization Selectivity, ACS Catal. 6 (2016) 7059–7070, https://doi.org/10.1021/acscatal.6b02128.
[62] R.J. Quann, L.A. Green, S.A. Tabak, F.J. Krambeck, Chemistry of olefin oligomerization over ZSM-5 catalyst, Ind. Eng. Chem. Res. 27 (1988) 565–570, https://doi.org/10.1021/ie00076a006.